43rd IEEE Conference on Decision and Control
December 14-17, 2004
Atlantis, Paradise Island, Bahamas

Real-Time Combustion Torque Estimation on a Diesel Engine Test Bench Using an adaptive Fourier Basis Decomposition

Jonathan Chauvin, Gilles Corde, Philippe Moulin, Michel Castagné, Nicolas Petit and Pierre Rouchon

Abstract— **We propose an estimator of the combustion torque on a Diesel Engine using as only sensor the easily available instantaneous crankshaft angle speed. The observer consists in an adaptive filter on the coefficients on the Fourier Basis decomposition designed on a physics-based time-varying model for the engine dynamics. Convergence is proven, using a Lyapounov function in both continuous and discrete cases. A test bench and development environment is presented. Performance is studied through simulations and real test bench experiments. Specific features of this observer are: a combustion model free dynamics expressed in angular time, and phase shift free reconstruction of the mass torque.**

I. Introduction

Performance and environmental requirements impose advance control strategies for automotive applications. In this context, controlling the combustion represents a key challenge. A first step is to control the combustion torque which characterizes the performance of the engine and is the result of various inputs such as injection quantity and timing, EGR (exhaust gas recirculation) rate ....

Ideally this torque could be measured using fast pressure sensors in each cylinder. Unfortunately their cost and reliability prevent these sensors from reaching commercial products. As a consequence an interesting problem is the design of a real-time observer for the combustion torque using the reliable and available instantaneous engine speed as only measurement.

Combustion torque determination by the measurement of the instantaneous engine speed has been addressed previously in the literature. Most of the proposed solutions have their foundation on a Direct or Indirect Fourier Transform for a black box model (see [7], [8], [5]). Other focus on a stochastic approach (see [6]) but the problem of real-time estimation is not addressed. Other approach such as mean indicated torque are also proposed (see [12] and [13] for example). Solving this first problem open the door to more exciting applications such as misfiring detection ([1] and [14]) and combustion analysis.

For the design of a combustion torque observer, we build a time-varying model based on the equations of mechanics underlying the role of time-varying inertia. This Fourier-based observer is validated experimentally (on the presented test bench) and theoretically (proof of the convergence). It is computationally tractable on a typical XPC Target (or DSpace system) embedded system capable of handling a 500 μs sampling time.

The contribution is as follows. In the Section II, we explain the engine dynamics. We describe the combustion torque observer design in Section III. In Section IV, we describe the experimental setup. Simulation and experimental results are presented in Section V. Future directions are given in Section VI.

J. Chauvin (corresponding author) is a PhD Candidate in Mathematics and Control, Centre Automatique et Systèmes, École des Mines de Paris, 60, bd St Michel, 75272 Paris, France chauvin@cas.ensmp.fr

G. Corde, P. Moulin and M. Castagné are with the Department of Engine Control in Institut Français du Pétrole, 1 et 4 Avenue de Bois Préau, 92852 Rueil Malmaison, France

N. Petit and P. Rouchon are with the Centre Automatique et Systèmes, École des Mines de Paris, 60, bd St Michel, 75272 Paris, France

II. Crankshaft dynamics

In this part, we briefly describe the dynamics of the system stressing out the role of the combustion torque, T_{comb}, also referred as the indicated torque. Following [10], the torque balance on the crankshaft can be written

$$T_{comb} - T_{mass} - T^*_{load} = 0 \tag{1}$$

where $T^*_{load} = T_{load} + T_{fric}$ is referred to "the extended load torque" and T_{load} and T_{fric} are known. The mass torque T_{mass} is the derivative of the kinetic energy E_{mass} of the moving masses in the engine as described in Figure 1.

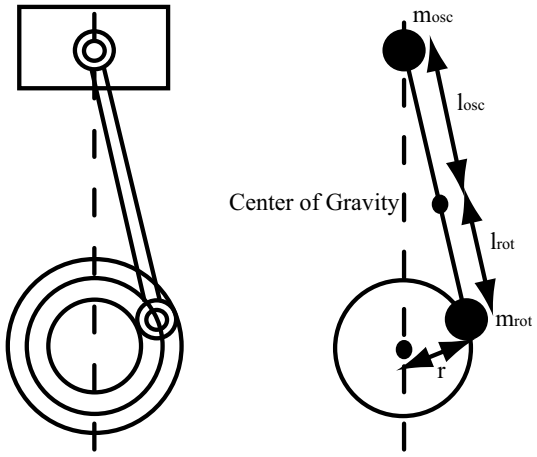

Fig. 1. Mass Model.

$$E_{mass} = \int_0^{2\pi} T_{mass} d\alpha = \frac{1}{2} J(\alpha) \dot{\alpha}^2$$

The mass torque T_{mass} can be expressed as

$$\frac{dE_{mass}}{dt} = T_{mass} \dot{\alpha}$$

with

$$J(\alpha) = m_{rot} r^2 + m_{osc} \sum_{j=1}^{4} (\frac{ds_j}{d\alpha})^2$$

the computation of the various elements of J are described in [4] and are usually perfectly known for a particular engine. $J(\alpha)$ is a periodic function in α over an engine cycle.

III. Fourier Decomposition : Continuous and Discrete-time cases

In this part, we propose to decompose the mass torque on a Fourier basis and make an adaptation of the coefficients. This observation technique is explained in a continuous time framework and then we move to the discrete time version of it which is more appropriate to real-time application.

A. Continuous Case

An energy balance yields

$$\frac{d}{d\alpha}(\frac{1}{2} J(\alpha)\dot{\alpha}^2) = T_{mass}(\alpha) \tag{2}$$

$T_{mass}(\alpha)$ is 4π-periodic, we can decompose it on a Fourier basis. Keeping the n_h first harmonics, we get the approximation:

$$T_{mass}(\alpha) \simeq a_0 + \sum_{i=1}^{n_h} (a_i \cos(i\frac{\alpha}{2}) + b_i \sin(i\frac{\alpha}{2}))$$

The dynamics reads

$$\frac{d\phi}{d\alpha} = a_0 + \sum_{i=1}^{n_h} (a_i \cos(i\frac{\alpha}{2}) + b_i \sin(i\frac{\alpha}{2}))$$

where $\phi(\alpha) = \frac{1}{2} J(\alpha)\dot{\alpha}^2$ is the kinetic energy of the system.

1) Reference model:

We have a 4π-periodic state-space model. The engine speed $\dot{\alpha}^2$ is the output and is referred to as y.

$$\left\{ \begin{array}{rcl} \frac{dx}{d\alpha} & = & \mathcal{M}(\alpha) x \\ y & = & C(\alpha) x \end{array} \right. \tag{3}$$

with

- the state $x = \left[\begin{array}{ccccccc} \phi & a_0 & a_1 & b_1 & \dots & b_{n_h} \end{array} \right]^T \in \mathcal{M}_{2(n_h+1),1}(\mathbb{R})$
- $\mathcal{M}(\alpha) = \left[\begin{array}{cc} 0 & M(\alpha) \\ 0 & 0 \\ \vdots & \vdots \\ 0 & 0 \end{array} \right] \in \mathcal{M}_{2(n_h+1),2(n_h+1)}(\mathbb{R})$
- $M(\alpha) = \left[\begin{array}{ccccc} 1 & \cos(\frac{\alpha}{2}) & \sin(\frac{\alpha}{2}) & \dots & \sin(n_h\frac{\alpha}{2}) \end{array} \right] \in \mathcal{M}_{1,2n_h+1}(\mathbb{R})$
- the observation matrix $C = \frac{2}{J(\alpha)} \left[\begin{array}{cccc} 1 & 0 & \dots & 0 \end{array} \right] \in \mathcal{M}_{1,2(n_h+1)}(\mathbb{R})$

2) Definition of the observer:

With this state-space model, we define a time-varying observer. The observer dynamics are:

$$\left\{ \begin{array}{rcl} \frac{d\hat{x}}{d\alpha} & = & \mathcal{M}(\alpha)\hat{x} - \mathcal{L}(\alpha)(\hat{y} - y) \\ \hat{y} & = & C(\alpha)\hat{x} \end{array} \right. \tag{4}$$

with

$$\mathcal{L}(\alpha) = \frac{J(\alpha)}{2} \left[\begin{array}{c} L_{ke} \\ L_{a_0} \\ L_{a_1} \cos(\frac{\alpha}{2}) \\ L_{b_1} \sin(\frac{\alpha}{2}) \\ \vdots \\ L_{a_{n_h}} \cos(n_h\frac{\alpha}{2}) \\ L_{b_{n_h}} \sin(n_h\frac{\alpha}{2}) \end{array} \right] \in \mathcal{M}_{2(n_h+1),1}(\mathbb{R})$$

where L_{ke} refers to the strictly positive gain on the kinetic energy, while $L_{a_0}, \dots, L_{b_{n_h}}$ are the strictly positive gains for the Fourier basis coefficients. For sake of simplicity we change notations through the following reordering. We define $\{f_k\}_{k\in\{0,2n_h\}}$ such that

$$\begin{array}{rcl} f_0(\alpha) & = & 1 \\ f_{2i-1}(\alpha) & = & \cos(i\frac{\alpha}{2}) \\ f_{2i}(\alpha) & = & \sin(i\frac{\alpha}{2}) \end{array}$$

and the strictly positive constants $\{l_k\}_{k\in[0,2n_h]}$ such that

$$\begin{array}{rcl} l_0 & = & L_{a_0} \\ l_{2i-1} & = & L_{a_i} \\ l_{2i} & = & L_{b_i} \end{array}$$

We have

$$\mathcal{L}(\alpha) = \frac{J(\alpha)}{2} \left[\begin{array}{c} L_{ke} \\ l_0 f_0(\alpha) \\ l_1 f_1(\alpha) \\ \vdots \\ l_{2n_h} f_{2n_h}(\alpha) \end{array} \right] \in \mathcal{M}_{2(n_h+1),1}(\mathbb{R})$$

To prove convergence of the state $\hat{x}$ of the observer (4) to the state x of the reference system (3), we exhibit a Lyapounov function and use LaSalle's theorem.

Let

- the error-state $\tilde{x} = x - \hat{x}$
- $D = \text{diag}(\begin{array}{cccc} 1 & \frac{1}{l_0} & \dots & \frac{1}{l_{2n_h}} \end{array})$

Classically, the error dynamics are:

$$\frac{d\tilde{x}}{d\alpha} = (\mathcal{M}(\alpha) - \mathcal{L}(\alpha)C(\alpha))\tilde{x} \tag{5}$$

3) Lyapounov function candidate:

We try as a Lyapounov function

$$V(\tilde{x}) = \frac{1}{2}\tilde{x}^T D \tilde{x} \tag{6}$$

By derivation of V with respect to α, we have

$$\begin{aligned}\frac{dV}{d\alpha} &= \tilde{x}^T D\frac{d\tilde{x}}{d\alpha} \text{ because } D \text{ is diagonal}\\ &= \tilde{x}^T D(\mathcal{M}(\alpha)\tilde{x} - \mathcal{L}(\alpha)(\hat{y}-y))\\ &= \tilde{x}^T D(\mathcal{M}(\alpha) - \mathcal{L}(\alpha)C(\alpha))\tilde{x}\\ &= -L\tilde{x}_1^2\\ &= -L(\phi-\hat{\phi})^2\end{aligned}$$

V is a Lyapounov function since it is continuously differentiable and satisfies

- $V(0)=0$ and $V(\tilde{x})>0$ for $\tilde{x}\in\mathbb{R}^{2(n_h+1)}\backslash\{0\}$
- $\frac{dV}{d\alpha}(\tilde{x})\leq 0$ in $\mathbb{R}^{2(n_h+1)}$

Lemma 1: The function V defined by (6) is a Lyapounov function for the error-state system (5).

4) Application of LaSalle's theorem:

Let $S_c(R)=\{\tilde{x}_f\in\mathbb{R}^{2(n_h+1)}/V(\tilde{x}_f)<R\}\subset\mathbb{R}^{2(n_h+1)}$. $S_c(R)$ is a compact set and is positively invariant with respect to the error dynamics (5). V is a continuously differentiable function such that $\frac{dV}{d\alpha}(\tilde{x}_f)\leq 0$ in $S_c(R)$. Let I_c be the largest invariant set in $\{\tilde{x}_f\in S_c(R)/\frac{dV}{d\alpha}(\tilde{x}_f)=0\}$. From LaSalle's theorem (see for instance [9] Theorem 4.4), every solution starting in $S_c(R)$ approaches I_c as $t\to\infty$.

5) Characterization of the invariant set:

We now try to characterize I_c. Let $\tilde{x}_f\triangleq\begin{bmatrix}\tilde{\phi}_f & \tilde{c}_f\end{bmatrix}^T$, where $\tilde{c}_f\triangleq\begin{bmatrix}\tilde{a}_{0,f} & \dots & \tilde{b}_{n_h,f}\end{bmatrix}$. We have

$$\tilde{x}_f\in\{\tilde{x}_f\in\mathbb{R}^{2(n_h+1)}/\frac{dV}{d\alpha}(\tilde{x}_f)=0\} \quad\Leftrightarrow\quad \tilde{\phi}_f=0$$

so

$$\begin{aligned}\{\tilde{x}_f\in\mathbb{R}^{2(n_h+1)}/\frac{dV}{d\alpha}(\tilde{x}_f)=0\} =\\ \{\begin{bmatrix}0 & \tilde{c}_f\end{bmatrix}^T/\tilde{c}_f\in\mathbb{R}^{2n_h+1}\}\end{aligned}$$

We apply the error dynamics to an element of

$$\{\begin{bmatrix}0 & \tilde{c}_f\end{bmatrix}^T/\tilde{c}_f\in\mathbb{R}^{2n_h+1}\}$$

To remain in I_c the variation of the first coordinate of the dynamics must be zero. So this implies

$$\forall\alpha\in\mathbb{R}\quad \tilde{c}_{f,0}+\sum_{i=1}^{n_h}\tilde{c}_{f,2i-1}\cos(i\frac{\alpha}{2})+\tilde{c}_{f,2i}\sin(i\frac{\alpha}{2})=0$$

Because the functions family $\{1,\cos(\frac{\alpha}{2}),\sin(\frac{\alpha}{2}),\ \dots,\ \cos(n_h\frac{\alpha}{2}),\sin(n_h\frac{\alpha}{2})\}$ is a linearly independent family of the set $\mathcal{C}^0(\mathbb{R}^+,\mathbb{R})$ of the continuous function of $\mathbb{R}$, the last equation yields $\{\tilde{c}_{f,i}=0\}_{i=0,\dots,2n_h}$. The set I_c is reduced to $\{0\}$. The observation error is asymptotically stable and the following results holds

Lemma 2: With V defined in (6), the largest set in $\{\tilde{x}_f\in\mathbb{R}^{2(n_h+1)}/\frac{dV}{d\alpha}(\tilde{x}_f)=0\}$ that is invariant by the dynamics of the System (3) is the null space

Proposition 1: The observer state defined in equation (4) converges toward the reference model state (3).

B. Discrete-time case

We move to the discrete time version of the observer which is more appropriate for real-time application.

1) Reference model:

In the discrete-time case, with the angular path $\Delta\alpha$ the dynamics are

$$\begin{aligned}\phi((n+1)\Delta\alpha)-\phi(n\Delta\alpha) =\\ \Delta\alpha(a_0+\sum_{i=1}^{n_h}(a_i\cos(in\Delta\frac{\alpha}{2})+b_i\sin(in\Delta\frac{\alpha}{2})))\end{aligned}$$

Let

- $\alpha_n=n\Delta\alpha$
- $x_n=x(\alpha_n)$
- $J_n=J(\alpha_n)$
- $\mathcal{M}_n=\mathcal{M}(\alpha_n)$
- $M_n=M(\alpha_n)$
- $C_n=C(\alpha_n)$
- $\forall i\in[0,\ 2n_h]\ f_i(n)=f_i(\alpha_n)$

with x, J, $\mathcal{M}$, M, C and $\{f_i\}_{i=0,\dots,2n_h}$ defined as in the previous subsection. The dynamics can be written as

$$\left\{\begin{array}{rcl}x_{n+1} &=& (I+\Delta\alpha\mathcal{M}_n)x_n\\ y_n &=& C_nx_n\end{array}\right. \tag{7}$$

2) Definition of the observer:

With this state-space model, we define a time-varying observer. We pose for the observer dynamics:

$$\left\{\begin{array}{rcl}\hat{x}_{n+1} &=& (I+\Delta\alpha\mathcal{M}_n)\hat{x}_n-\mathcal{L}_n(\hat{y}_n-y_n)\\ \hat{y}_n &=& C_n\hat{x}_n\end{array}\right. \tag{8}$$

with

$$\mathcal{L}_n=\frac{\Delta\alpha J_n}{2}\begin{bmatrix}L_{ke}\\ L_{a_0}\\ L_{a_1}\cos(\frac{\alpha_n}{2})\\ L_{b_1}\sin(\frac{\alpha_n}{2})\\ \vdots\\ L_{a_{n_h}}\cos(n_h\frac{\alpha_n}{2})\\ L_{b_{n_h}}\sin(n_h\frac{\alpha_n}{2})\end{bmatrix}\in\mathcal{M}_{2(n_h+1),1}(\mathbb{R}) \tag{9}$$

With the notations introduced in the previous subsection

$$\mathcal{L}_n=\frac{\Delta\alpha J_n}{2}\begin{bmatrix}L_{ke}\\ l_0f_0(n)\\ l_1f_1(n)\\ \vdots\\ l_{2n_h}f_{2n_h}(n)\end{bmatrix}\in\mathcal{M}_{2(n_h+1),1}(\mathbb{R}) \tag{10}$$

To prove the convergence of the observer (8) to the reference model (7) , we explicit a Lyapounov function and use LaSalle's theorem.

3) Lyapounov function candidate:

We try as a Lyapounov function

$$V(\tilde{x}_n)=\frac{1}{2}\tilde{x}_n^TD\tilde{x}_n \tag{11}$$

We now compute $\Delta V(\tilde{x}_{n+1})=V(\tilde{x}_{n+1})-V(\tilde{x}_n)$. First

$$\begin{aligned}\tilde{x}_{n+1}-\tilde{x}_n &= \Delta\alpha\mathcal{M}_n\tilde{x}_n-\mathcal{L}_n(\hat{y}_n-y_n)\\ &= \Delta\alpha\mathcal{M}_n\tilde{x}_n-\mathcal{L}_nC_n\tilde{x}_n\\ &= (\Delta\alpha\mathcal{M}_n-\mathcal{L}_nC_n)\tilde{x}_n\\ &\triangleq \Xi_n\tilde{x}_n\end{aligned}$$

The error dynamics are:

$$\tilde{x}_{n+1} = (I + \Xi_n)\tilde{x}_n \tag{12}$$

Then

$$\begin{aligned}\Delta V(\tilde{x}_n) &= V(\tilde{x}_{n+1}) - V(\tilde{x}_n) \frac{1}{2}\tilde{x}_{n+1}^T D \tilde{x}_{n+1} - \frac{1}{2}\tilde{x}_n^T D \tilde{x}_n \\ &= \frac{1}{2}\tilde{x}_n^T (I+\Xi_n)^T D (I+\Xi_n)\tilde{x}_n - \frac{1}{2}\tilde{x}_n^T D \tilde{x}_n\end{aligned}$$

We have

$$\Delta V(\tilde{x}_n) = -\frac{1}{2}\tilde{x}_n^T \Omega_n \tilde{x}_n \tag{13}$$

with

$$\Omega_n \triangleq -\Xi_n^T D \Xi_n - \Xi_n^T D - D\Xi_n$$

To check negativeness of $\Delta V(\tilde{x}_n)$, we have to check positiveness of Ω_n. On the one hand

$$\Xi_n = \Delta\alpha \begin{bmatrix} -L_{ke} & f_0(n) & f_1(n) & \dots & f_{2n_h}(n) \\ -l_0 f_0(n) & 0 & 0 & \dots & 0 \\ -l_1 f_1(n) & 0 & 0 & \dots & 0 \\ \dots & 0 & 0 & \dots & 0 \\ -l_{2n_h} f_{2n_h}(n) & 0 & 0 & \dots & 0 \end{bmatrix}$$

And thus

$$\Omega_n = (\Delta\alpha)^2 \begin{bmatrix} -\omega_n & L_{ke} f_0(n) & \dots & L_{ke} f_{2n_h}(n) \\ L_{ke} f_0(n) & & & \\ \dots & & -M_n^T M_n & \\ L_{ke} f_{2n_h}(n) & & & \end{bmatrix}$$

where $\omega_n \triangleq L_{ke}^2 - \frac{2}{\Delta\alpha} L_{ke} + \sum_{i=0}^{2n_h} l_i f_i^2(n)$. Let $u_n \triangleq L_{ke} M_n^T$

$$\Omega_n = \begin{bmatrix} -\omega_n & u_n^T \\ u_n & -M_n^T M_n \end{bmatrix}$$

Let

$$\mathbb{R}\times\mathbb{R}^{2n_h+1} \ni (x_1, x_2) \mapsto \phi(x_1, x_2) = \begin{bmatrix} x_1 \\ x_2 \end{bmatrix}^T \Omega_n \begin{bmatrix} x_1 \\ x_2 \end{bmatrix}$$

Then $\forall (x_1,\ x_2)$

$$\begin{aligned}\phi(x_1, x_2) &= \begin{bmatrix} x_1^T & x_2^T \end{bmatrix} \begin{bmatrix} -\omega_n x_1 + u_n^T x_2 \\ u_n x_1 - M_n^T M_n x_2 \end{bmatrix} \\ &= -x_1^T \omega_n x_1 + x_1^T u_n^T x_2 + x_2^T u_n x_1 \\ &\quad -x_2^T M_n^T M_n x_2 \\ &= -\omega_n x_1^2 + 2 x_1 u_n^T x_2 - x_2^T M_n^T M_n x_2\end{aligned}$$

Then

$$\min_{x_1} \phi(x_1, x_2) = x_2^T (\frac{1}{\omega_n} u_n u_n^T - M_n^T M_n) x_2$$

because for a given x_2, the minimum of the quadratic form in x_1 is obtained for

$$x_1 = \frac{1}{\omega_n} u_n^T x_2$$

Substituting u_n with its definition, we get

$$\min_{x_1} \phi(x_1, x_2) = x_2^T (\frac{L_{ke}^2}{\omega_n} - 1) M_n^T M_n x_2$$

Substituting ω_n with its value we obtain that a necessary and sufficient condition for the matrix Ω_n to be definite positive is

$$L_{ke} > \frac{\Delta\alpha}{2} \sum_{i=0}^{2n_h} l_i f_i^2(n)$$

In short, with the initial notations of the observers gains as given in Equation (9), Ω_n is positive iff

$$L_{ke} > \frac{\Delta\alpha}{2} (L_{a_0} + \sum_{i=0}^{n_h} L_{a_i} \cos(i\frac{\alpha_n}{2})^2 + L_{b_i} \sin(i\frac{\alpha_n}{2})^2) \tag{14}$$

Under this hypothesis V is a Lyapounov function since

- $V(0) = 0$ and $V(\tilde{x}) > 0$ for $\tilde{x} \in \mathbb{R}^{2(n_h+1)} \backslash \{0\}$
- $\Delta V(\tilde{x}_n) \leq 0$ in $\mathbb{R}^{2(n_h+1)}$

Lemma 3: Under the assumption (14), the function V defined by (11) is a Lyapounov function for the error-state system.

4) Decomposition as N subsystems:
The variation of V (ΔV) depends on the sample time n, so we can not use the discrete version of LaSalle's Theorem we used in the continuous case. However the dynamics of the error over a time interval of the form $[k, k+N]$, $k \in [1, N]$, are stationary. This fact leads us to consider a collection of N subsystems $\{\mathcal{S}_k\}_{k=1,\dots,N}$ that are N shifted down-sampled versions of the original system. We then apply LaSalle's Theorem for each subsystem and conclude on the convergence.

For all $k \in [1, N]$, the error dynamics over $[k, k+N]$ are

$$(\mathcal{S}_k) \begin{cases} \tilde{\eta}_{n+1} &= \tilde{\Phi}(k+N, k)\tilde{\eta}_n \\ \tilde{\eta}_n &= \tilde{x}_{k+nN} \end{cases} \tag{15}$$

with $\tilde{\Phi}$ the transition matrix of the error

$$\tilde{\Phi}(k+N, k) = (I + \Xi_{k+N-1}) \dots (I + \Xi_k)$$

We compute (with V defined in (11))

$$\begin{aligned} V(\tilde{\eta}_{n+1}) - V(\tilde{\eta}_n) &= V(\tilde{x}_{k+(n+1)N}) - V(\tilde{x}_{k+nN}) \\ &= \sum_{j=0}^{N-1} (V(\tilde{x}_{k+nN+j+1}) - V(\tilde{x}_{k+nN+j})) \\ &= \sum_{j=0}^{N-1} \Delta V(\tilde{x}_{k+nN+j}) \\ &\leq 0 \ \text{ because} \\ &\quad \forall j = 0, \dots, N-1 \ \ \Omega_{k+nN+j} \geq 0 \end{aligned}$$

The function V is a Lyapounov function for the system described by (15) because

- $V(0) = 0$ and $V(\tilde{\eta}) > 0$ for $\tilde{\eta} \in \mathbb{R}^{2(n_h+1)} \backslash \{0\}$
- $V(\tilde{\eta}_{n+1}) - V(\tilde{\eta}_n) \leq 0$

Lemma 4: The function V defined in (11) is a Lyapounov function for the error-state system $\mathcal{S}_k$ described by (15).

5) Application of LaSalle's theorem:
Let $S_{d,k}(R) = \{\tilde{x}_f \in \mathbb{R}^{2(n_h+1)} / V(\tilde{x}_f) < R\} \subset \mathbb{R}^{2(n_h+1)}$. $S_{d,k}(R)$ is a compact set and is positively invariant with respect to the error dynamics (15). V is a differentiable function such that $V(\tilde{\Phi}(k+N,k)\tilde{x}_f) - V(\tilde{x}_f) \leq 0$ in $S_{d,k}(R)$. Let $I_{d,k}$ be the largest invariant set in $\{\tilde{x}_f \in S_{d,k}(R) / V(\tilde{\Phi}(k+N,k)\tilde{x}_f) - V(\tilde{x}_f) = 0\}$. From LaSalle's theorem (see for instance [11] §2.6), every solution starting in $S_{d,k}(R)$ approaches $I_{d,k}$ as $n \to \infty$.

6) Characterization of the invariant set:
We now try to characterize $I_{k,d}$. Let $\tilde{\eta}_{k,f} \triangleq \begin{bmatrix} \tilde{\phi}_{k,f} & \tilde{c}_{k,f} \end{bmatrix}^T$ where $\tilde{c}_{k,f} \triangleq \begin{bmatrix} \tilde{a}_{0,k,f} & \dots & \tilde{b}_{n_h,k,f} \end{bmatrix}$. We have

$$\begin{aligned}
&\{\tilde{\eta}_{k,f} \in \{\tilde{x}_f \in S_{d,k}(R) / V(\tilde{\Phi}(k+N,k)\tilde{x}_f) - V(\tilde{x}_f) = 0\}\} \\
&\Leftrightarrow V(\tilde{\Phi}(k+N,k)\tilde{\eta}_{k,f}) - V(\tilde{\eta}_{k,f}) = 0 \\
&\Leftrightarrow \textstyle\sum_{i=k}^{k+N} V(\tilde{\Phi}(i+1,k)\tilde{\eta}_{k,f}) - V(\tilde{\Phi}(i,k)\tilde{\eta}_{k,f}) = 0 \\
&\Leftrightarrow \tilde{\eta}_{k,f}^T W_k \tilde{\eta}_{k,f} = 0
\end{aligned}$$

with

$$W_k \triangleq \sum_{i=0}^{N-1} \tilde{\Phi}(k+i,k)^T \Omega_{k+i} \tilde{\Phi}(k+i,k)$$

Let $\tilde{\Phi}(k+i,k)\tilde{\eta}_{k,f} \triangleq \begin{bmatrix} \tilde{\phi}_{k_i,f} & \tilde{c}_{k_i,f} \end{bmatrix}^T$. Then

$$\begin{aligned}
&\{\tilde{\eta}_{k,f} \in \{\tilde{x}_f \in S_{d,k}(R) / V(\tilde{\Phi}(k+N,k)\tilde{x}_f) - V(\tilde{x}_f) = 0\}\} \\
&\Leftrightarrow \tilde{\eta}_{k,f}^T W_k \tilde{\eta}_{k,f} = 0 \\
&\Leftrightarrow \forall i \in [\,0,\ N-1], \\
&\tilde{\eta}_{k,f}^T \tilde{\Phi}(k+i,k)^T \Omega_{k+i} \tilde{\Phi}(k+i,k) \tilde{\eta}_{k,f} = 0 \\
&\Leftrightarrow \forall i \in [\,0,\ N-1],\ \begin{cases} \tilde{\phi}_{k_i,f} = \frac{1}{\omega_i} u_i^T \tilde{c}_{k_i,f} \\ M_i \tilde{c}_{k_i,f} = 0 \end{cases} \\
&\Leftrightarrow \forall i \in [\,0,\ N-1],\ \begin{cases} \tilde{\phi}_{k_i,f} = 0 \\ M_i \tilde{c}_{k_i,f} = 0 \end{cases}
\end{aligned}$$

because $u_i = L_{ke} M_i^T$. Moreover, by computing by induction the $\tilde{c}_{k_i,f}$, we have $\tilde{c}_{k_i,f} = \tilde{c}_{k,f}$. We can summarize the previous equivalences by:

$$\begin{aligned}
&\{\tilde{\eta}_{k,f} \in \{\tilde{x}_f \in S_{d,k}(R) / V(\tilde{\Phi}(k+N,k)\tilde{x}_f) - V(\tilde{x}_f) = 0\}\} \\
&\Leftrightarrow \begin{cases} \Gamma_k \tilde{c}_{k,f} = 0 \\ \tilde{\phi}_{k,f} = 0 \end{cases}
\end{aligned}$$

with

$$\Gamma_k = \begin{bmatrix} 1 & 1 & \dots & 1 \\ \cos(\frac{\alpha_k}{2}) & \cos(\frac{\alpha_{k+1}}{2}) & \dots & \cos(\frac{\alpha_{k+N-1}}{2}) \\ \sin(\frac{\alpha_k}{2}) & \sin(\frac{\alpha_{k+1}}{2}) & \dots & \sin(\frac{\alpha_{k+N-1}}{2}) \\ \vdots & \vdots & \vdots & \vdots \\ \sin(n_h \frac{\alpha_k}{2}) & \sin(n_h \frac{\alpha_{k+1}}{2}) & \dots & \sin(n_h \frac{\alpha_{k+N-1}}{2}) \end{bmatrix}^T$$

Again the functions family $\{1, \cos(\frac{\alpha}{2}), \dots, \sin(n_h \frac{\alpha}{2})\}$ is a linearly independent family of $\mathcal{C}^0(\mathbb{R},\mathbb{R})$. So the matrix Γ_k defined above has full rank if $Card(\{\alpha_i \equiv 0 \mod (4\pi)\}_{i=1..N}) = 2n_h + 1$.[1] Indeed, if we pose $\Sigma_{4\pi} = \{\alpha_i /\ 0 < i < \frac{4\pi}{\Delta\alpha}\}$, the previous condition is false iff

$$\begin{cases} \alpha_{2n_h+1} \notin [0, 4\pi] \\ \alpha_{2n_h+1} \equiv 0 \mod (4\pi) \in \Sigma_{4\pi} \end{cases}$$

A sufficient condition is trivially

$$\alpha_{2n_h+1} < 4\pi$$

Under this assumption,

$$\begin{aligned}
&\{\tilde{\eta}_{k,f} \in \{\tilde{x}_f \in S_{d,k}(R) / V(\tilde{\Phi}(k+N,k)\tilde{x}_f) - V(\tilde{x}_f) = 0\}\} \\
&\Rightarrow \tilde{\eta}_{k,f} = 0
\end{aligned}$$

The set $I_{d,k}$ is reduced to $\{0\}$ and the following result holds

Lemma 5: With V defined in (11), the largest set $\{\tilde{x}_f \in S_{d,k}(R) / V(\tilde{\Phi}(k+N,k)\tilde{x}_f) - V(\tilde{x}_f) = 0\}$ which is invariant by the dynamics of the (15) is the null space

7) Conclusion on the observer convergence:
For all $k \in [1, N]$, the system (15) is asymptotically stable so all the $(\tilde{x}_{k+iN})_{i \in \mathbb{N}}$ converge to 0, it is also the case for the error $(\tilde{x}_i)_{i \in \mathbb{N}}$ and the following results yield

Lemma 6: With V defined by (11), the largest set $\{\tilde{x}_f \in \mathbb{R}^{2(n_h+1)} / \Delta V(\tilde{x}_f) = 0\}$ which is invariant by the dynamics of the (7) is the null space

Proposition 2: The discrete-time observer state defined in equation (8) converges toward the discrete-time reference model state (7).

IV. Experimental Setup for Control Design

In this paper we deal with a 4-cylinder Diesel engine. This reference system is simulated using a Chmela combustion model [3] (nondimensional combustion model that relies on the concept of mixing controlled combustion avoiding the detailed description of the individual mixture formation and fuel oxidation process) coded in Simulink.

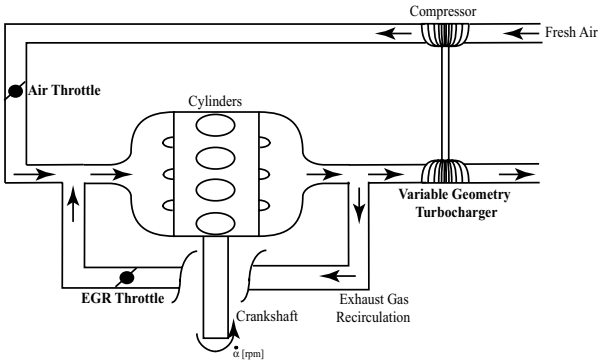

Fig. 2. Engine Scheme.

In our work, we try to restrict most of the design and tuning work to the simulation environment. This reduces the costly work on the engine test bench.

This HiL (Hardware in the Loop) platform is easily transferred to a fast prototyping system. The same code is kept and implemented in the control system to be tested on the test bench.

Typically 1 second of engine simulation is computed in 30 seconds on a 1 GHz Pentium based computer.

[1] In practice when a 6^o angle step is used, one may not use more that 60 harmonics, otherwise this last condition fails.

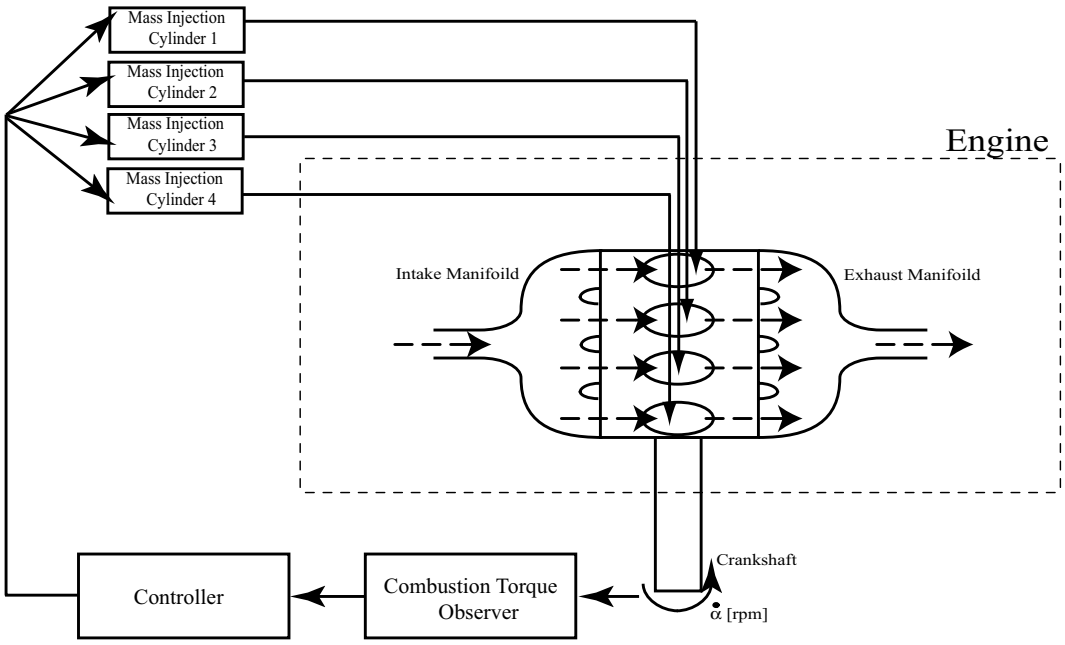

Fig. 3. Global Scheme.

V. Simulation and Experimental Results

A. Choice of the number of harmonics

In all the previous section, we use a general parameter n_h corresponding to the number of harmonics used to reconstruct the signal. The number of harmonics must be large enough to estimate the signal, but on the other hand the more harmonics we have, the more tedious the tuning phase is. Figure 4 shows reconstructed harmonics expansions using various number of harmonics n_h. We see that we need at least five harmonics to represent the signal well.

B. Observer Tuning

Without any methodology, the tuning of the parameters of the observer is tricky. We have $n_h + 2$ parameters to tune (as there is apparently no reason to differentiate the $\cos$ and the $\sin$ terms for the same frequency). Here, we propose a methodology that leads to the tuning of only three parameters whatever the choice of n_h. We choose $L_{a_i} \triangleq L_{b_i} \triangleq iL_{ref}$. We still have three parameters to pick (L_{ke}, L_{a_0} and L_{ref}). L_{ke} is the $\dot{\alpha}^2$ feedback term and is chosen with respect to the expected noise on the instantaneous engine speed $\dot{\alpha}$ measurement. L_{a_0} is the feedback term that assures convergence of the constant term in the harmonics expression. It is chosen with respect to the desired speed of convergence compared to the engine speed. The last parameter can be ranged by rewriting (14)

$$L_{ref} < \frac{2}{n_h(n_h-1)}\left(\frac{2}{\Delta\alpha}L_{ke} - L_{a_0}\right) \qquad (16)$$

Nevertheless, the choice of L_{ke} is difficult since it is the compromise between precision and robustness. With this choice of parametrization, convergence is guaranteed.

C. Results and Comments

In the next figures, we have the comparison of the performance of the observer presented in [2], and the observer presented here. This last observer relies on a pole-placement for a extended state space model of the engine that assumes $\dot{x}_2 = 0$. Though giving qualitatively interesting results it suffers from a lag and a lack of accuracy. T_{mass} is estimated through our observer, then T_{comb} is computed by adding T_{mass} and T^*_{load} according to (1).

1) Simulation results:

We present a simulation corresponding to a set point:

- Engine Speed : 1000 rpm
- BMEP (Brake Mean Effective Pressure) : 5 bar

To simulate the unbalance, we introduce offsets in the mass injected in each cylinder.

- Cylinder 1: 10% of the reference mass
- Cylinder 2: 0% of the reference mass
- Cylinder 3: 0% of the reference mass
- Cylinder 4: -20% of the reference mass

In Figure 5 the set point is a low engine speed and a low load. This point is very interesting because it represents where the driver feels internal loads and vibrations most. Correcting the unbalance at this points increases the driver's comfort.

2) Experimental Results:

Figures 6 and 7 display the result of the estimator on experimental data. We reconstruct the combustion torque from the bench with the in-cylinder pressure and we test the observer on the flywheel velocity measurement. The setting point is not the same as the simulation one.

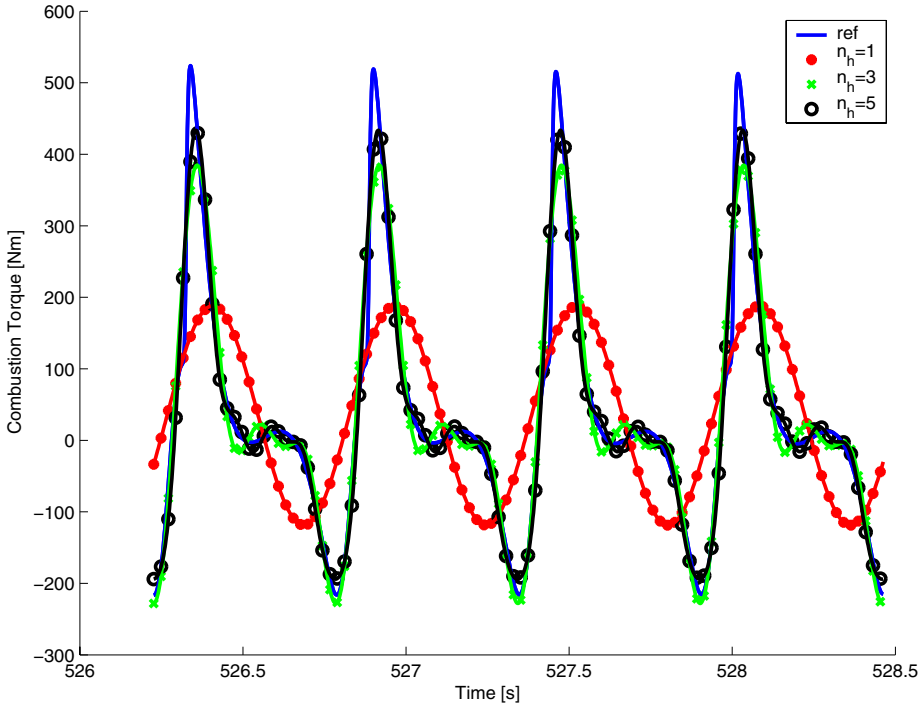

Fig. 4. Decomposition of the mass torque T_{mass} (1500 rpm, 2 bar), comparisons between the reference signal and its reconstructed version through harmonic expansion.

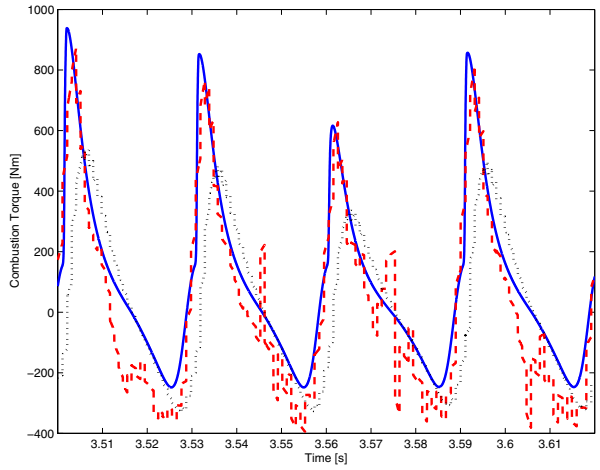

Fig. 5. Combustion torque on simulation (1000 rpm, 5 bar). bold (blue) : reference combustion torque, dashed (red) : combustion torque estimated by the the presented filter, dotted (black) : combustion torque estimated by pole placement as in [2].

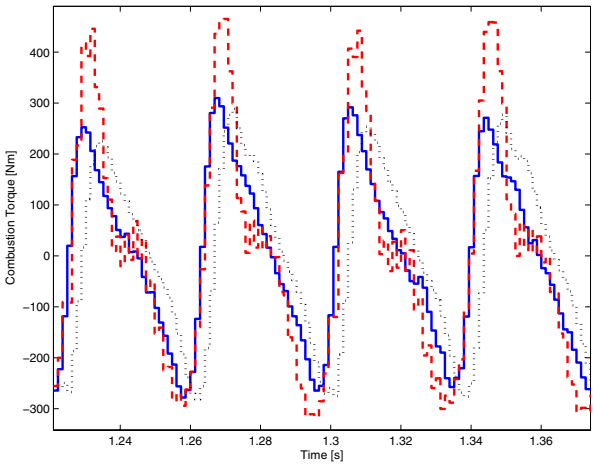

Fig. 6. Combustion torque on the test bench (800 rpm, 2 bar). bold (blue) : reference combustion torque, dashed (red) : combustion torque estimated by the presented filter, dotted (black) : combustion torque estimated by pole placement as in [2].

3) Comments: The decomposition of the Fourier basis seems to be relevant on this application. Even if the number of harmonics needed to recompose the signal is high (5 in the presented results), a simple methodology allows us to reduce the number of parameters to tune to only three. In practice though, the bottleneck is the low sampling rate. When few samples are available during a cycle (typically 120), adaptation of the coefficients can reveal problematic. This imposes an upper limitation on the number of harmonics. Moreover, this method is very sensitive to the noise on the 6^o measurement (due to the imperfection of the flywheel and the angular encoder). This noise is twofold: classic noise on the value of the engine speed and inaccurate synchronization on the 6^o flywheel. The harmonic decomposition of the signal assumes perfect periodicity of the instantaneous engine speed signal and

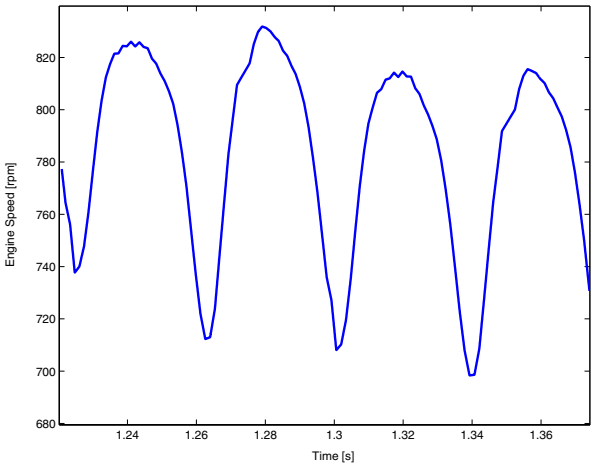

Fig. 7. Engine Speed $[rpm]$ on the test bench used as input for the observer

yields erroneous adaptation when synchronization noise on the angle is present (unlikely in practice, since the encoder is high quality and either based on optical or mechanical technology). As usual there is a tradeoff between the requested accuracy and the noise on the measurements.

In Figure 5 results from simulation are given. The overall shape of the signal is well reconstructed. No phase shift is present (by contrast the pole placement observer has a 18^o phase shift). The maximums are accurate, in facts the obtained values almost reach the values of the off-line best harmonic approximation in Figure 4. Noise is present on the lower part of the signals. It is due to the previously exposed issue. In the simulator there is a mismatch between the time-samples and the angular samples. This mismatch is particularly important when the angular speed reaches its maximum. This is the case when the torque reaches zero. This phenomenon can be avoided by reducing the time sample, but we found it illustrative not to do so, since in practice such errors are representative of encoders noise. In the presented simulations the time-sample is $10\mu s$ which corresponds (with fluctuations due to the variable engine speed) to $1/100$ of the angular step.

In Figure 6 results from the test bench are given. The same observer is used. The engine speed is given in Figure 7. Results are satisfactory. The noise on the test bench signal induces errors that are different from the simulated ones. More precisely, maximums are over estimated, but their relative values are consistent. Noise at the maximum of the engine speed is still present but attenuated. Most importantly no phase shift is induced.

VI. Conclusion and Future Work

The results of the presented adaptive Fourier basis decomposition observer are good. As is, robustness of the observer with respect to engine speed noises is satisfactory but could be improved further. This is not an easy problem though, since filtering of the input signals could help, but phase shifts are not acceptable.

In the context of combustion real-time control, this observer is a handy tool. It does not suffer from any phase shift, and can thus be used in a closed loop controller of the fuel injectors. This is the long term goal of our work.

Moreover this observer is easily transposed to various engine speeds and loads. Its dynamics are expressed in angular time scale and do not require any model for the combustion process. Theoretically, the gains do not need to be updated when the set-point is changed. However, due to the encoder structure, noise is not completely set-point independent, so in practice some re-tuning is required. We are currently investigating this point in an exhaustive test campaign on the test bench (engine speed ranging from 800 to 4000 rpm, load ranging from 2 to 14 bar).

References

[1] J. Ball, J. Bowe, C. Stone, and P. McFadden, "Torque estimation and misfire detection using block angular acceleration," in *Proc. of SAE Conference*, 2000.

[2] J. Chauvin, G. Corde, P. Moulin, M. Castagné, N. Petit, and P. Rouchon, "Observer design for torque balancing on a di engine," in *Proc. of SAE Conference*, 2004.

[3] F. Chmela and G. Orthaber, "Rate of heat release prediction for direct injection diesel engines based on purely mixing controlled combustion," in *Proc. of SAE Conference*, no. 1999-01-0186, 1999.

[4] H. Fehrenbach, "Model-based combustion pressure computation through crankshaft angular acceleration analysis," *Proceedings of* 22^{nd} *International Symposium on Automotive Technology*, vol. I, 1990.

[5] S. Ginoux and J. Champoussin, "Engine torque determination by crankangle measurements: State of art, future prospects," in *Proc. of SAE Conference*, no. 970532, 1997.

[6] P. Gyan, S. Ginoux, J. Champoussin, and Y. Guezennec, "Crankangle based torque estimation: Mechanistic/stochastic," in *Proc. of SAE Conference*, 2000.

[7] L. Jianqiu, Y. Minggao, Z. Ming, and L. Xihao, "Advanced torque estimation and control algorithm of diesel engines," in *Proc. of SAE Conference*, 2002.

[8] ——, "Individual cylinder control of diesel engines," in *Proc. of SAE Conference*, no. 2002-01-0199, 2002.

[9] H. Khalil, *Nonlinear Systems*. Prentice-Hall, Inc., 1992.

[10] U. Kiencke and L. Nielsen, *Automotive Control Systems For Engine, Driveline, and Vehicle*, Springer, Ed. SAE Internationnal, 2000.

[11] J. LaSalle, *The Stability and Control of Discrete Processes*, Springer-Verlag, Ed., 1986.

[12] G. Rizzoni, "Estimate of indicated torque from crankshaft speed fluctuations: A model for the dynamics of the IC engine," vol. 38, pp. 169–179, 1989.

[13] G. Rizzoni and F. Connolly, "Estimate of IC engine torque from measurment of crankshaft angular position," in *Proc. of SAE Conference*, 1993.

[14] J. Williams, "An overview of misfiring cylinder engine diagnostic techniques based on crankshaft angular velocity measurements," in *Proc. of SAE Conference*, 1996.